

Supporting Information

Organolanthanide η^1 - and η^5 -pyrrolyl half-sandwich compounds: synthesis, structures, and magnetic properties

Yeye She,^a Yanhua Lu,^a Chaohong Jia,^a Yahong Li,^{*a} Yi-Quan Zhang^{*b} and Jin-lei Yao^{*c}

^aCollege of Chemistry, Chemical Engineering and Materials Science, Soochow University, Suzhou 215123, P. R. China. E-mail: liyahong@suda.edu.cn

^bJiangsu Key Laboratory for NSLSCS, School of Physical Science and Technology, Nanjing Normal University, Nanjing 210023, China. E-mail: zhangyiquan@njnu.edu.cn

^cJiangsu Key Laboratory of Micro and Nano Heat Fluid Flow Technology and Energy Application, School of Physical Science and Technology, Suzhou University of Science and Technology, Suzhou 215009, China. E-mail: jlyao@usts.edu.cn

Contents

1. General methods.....	2
2. Computational details	3
3. Synthesis of the H₂L ligand.....	8
4. Structures and crystallographic data of complexes	9
4.1. Molecular structures of complexes	9
4.2. Bond lengths of complexes	12
4.3. Bond angles of complexes	13
5. SHAPE program details for 1, 2, and 3·4Tol.....	17
6. The ac magnetic susceptibility measurement of complexes 1 and 2.	18
7. The M-H plots of complexes 1-4	20
8. The Curie-Weiss law fits of complexes 1-4.....	21

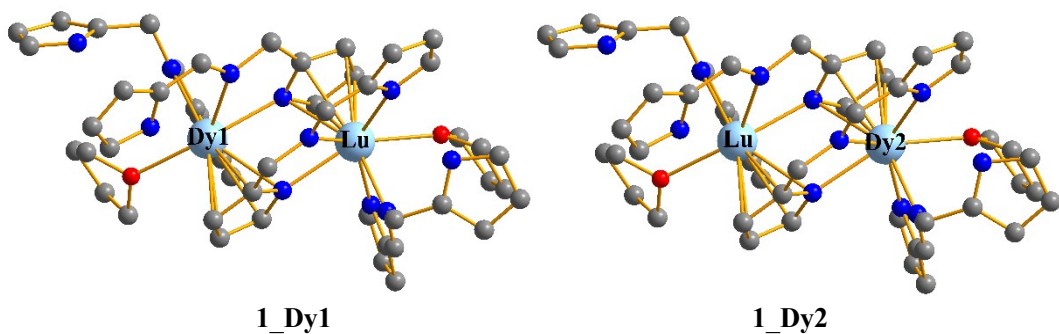
1. General methods

All the reactions were performed in a N₂ filled Vigor glove box. THF, hexane and toluene were dried over purple sodium benzophenone ketyl and stored with 4 Å molecular sieves. Deuterochloroform was dried over CaH₂ before distilled under vacuum and stored with 4 Å molecular sieves. ¹H NMR spectra were recorded at the ambient temperature on Bruker Avance-III 300 MHz. Elemental analyses for C, H and N were carried out on a Perkin-Elmer 2400 analyzer. The crystals data collections were performed from a Bruker AXS three-circle goniometer with a CCD detector at low temperature. We used OLEX-2 to analyze the crystal structures. The dc analyses were performed on polycrystalline samples wrapped in a polyethylene membrane (prepared in an inert atmosphere) under a field at 1000 Oe between 2 and 300 K. The crystal data were collected with a Bruker AXS three-circle goniometer with a CCD detector at low temperature, and the crystal structures were analysed using OLEX2 crystal analysis software. The crystallographic information file (CIF) was deposited with the Cambridge Crystallographic Data Centre deposition numbers CCDC 2213167 (**1·2THF**), 2213168 (**2**), and 2258043 (**3·4Tol**).

2. Computational details

Both of binuclear complexes **1** and **2** have two types of magnetic center Dy^{III} or Ho^{III} ions. Complete-active-space self-consistent field (CASSCF) calculations on two types of Ln^{III} fragments indicated as **1_Dy1**, **1_Dy2**, **2_Ho1** and **2_Ho2** for complexes **1** and **2** (see Figure S1) on the basis of single-crystal X-ray determined geometry have been carried out with OpenMolcas^{S1} program package. Each of individual Ln^{III} fragments in complexes **1** and **2** was calculated keeping the experimentally determined structures of the corresponding compounds while replacing the neighboring Ln^{III} ions with diamagnetic Lu^{III} .

The basis sets for all atoms are atomic natural orbitals from the ANO-RCC library: ANO-RCC-VTZP for Dy^{III} or Ho^{III} ; VTZ for close O, C and N; VDZ for distant atoms. The calculations employed the second order Douglas-Kroll-Hess Hamiltonian, where scalar relativistic contractions were taken into account in the basis set and the spin-orbit couplings were handled separately in the restricted active space state interaction (RASSI-SO) procedure.^{S2,S3} Active electrons in 7 active orbitals include all *f* electrons CAS(9 in 7) for Dy^{III} and CAS(10 in 7) for Ho^{III} in the CASSCF calculations. To exclude all the doubts, we calculated all the roots in the active space. We have mixed the maximum number of spin-free states which was possible with our hardware (all from 21 sextets, 128 from 224 quadruplets and 130 from 490 doublets for Dy^{III} ; all from 35 quintuplets, 150 from 210 triplets, 120 from 196 singles for Ho^{III}). SINGLE_ANISO^{S4-S6} program was used to obtain the energy levels, *g* tensors, magnetic axes, *et al.* based on the above CASSCF/RASSI-SO calculations.



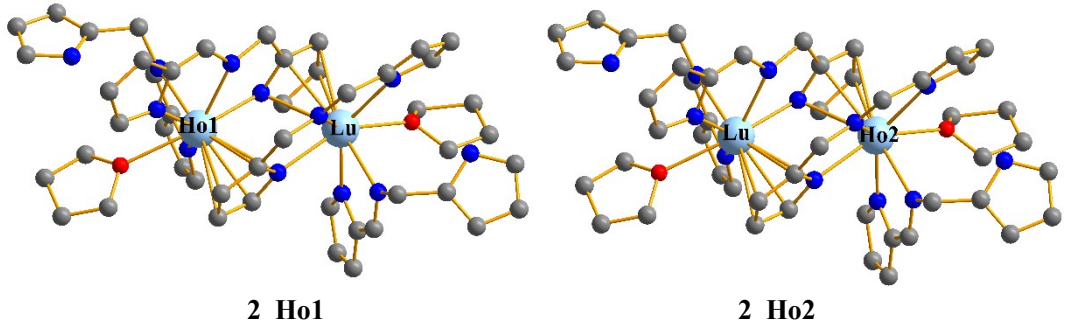


Figure S1. Calculated model structures of individual Ln^{III} fragments in complexes **1** and **2**; H atoms are omitted for clarity.

Table S1. Calculated energy levels (cm^{-1}), \mathbf{g} (g_x, g_y, g_z) tensors and predominant m_J values of the lowest eight or nine spin-orbit states of individual Ln^{III} fragments of complexes **1** and **2** using CASSCF/RASSI-SO with OpenMolcas.

KDs	1_Dy1			1_Dy2		
	<i>E</i>	\mathbf{g}	m_J	<i>E</i>	\mathbf{g}	m_J
1	0.0	0.003 0.005 19.587	$\pm 15/2$	0.0	0.369 0.428 17.795	$\pm 15/2$
2	113.4	0.039 0.058 16.764	$\pm 13/2$	103.9	0.027 0.043 16.735	$\pm 13/2$
3	251.4	1.488 2.940 12.607	$\pm 11/2$	236.4	1.711 3.718 12.078	$\pm 11/2$
4	310.4	2.549 6.039 10.690		292.4	9.952 6.146 2.168	
5	364.3	0.901 1.328 16.822		361.8	0.841 1.524 15.238	
6	391.6	1.438 2.479 12.430		381.4	1.138 1.803 14.457	
7	472.7	0.781 1.617 14.798		462.2	0.951 1.292 14.689	
8	514.2	0.369 0.428 17.795		518.8	0.125 0.233 18.043	
	2_Ho1			2_Ho2		
1	<i>E</i>	\mathbf{g}	m_J	<i>E</i>	\mathbf{g}	m_J
	0.0	0.000 0.000	± 8	0.0	0.000 0.000	± 8
	2.4	18.360		3.6	18.196	

2	84.6			74.1		
3	105.8	0.000		100.1	0.000	
	119.9	0.000		116.0	0.000	
	6.525	6.525			6.181	
4	161.8	0.000		159.3	0.000	
	183.3	0.000		190.9	0.000	
	5.161	5.161			8.281	
5	187.2	0.000		195.4	0.000	
	215.4	0.000		220.6	0.000	
	1.982	1.982			6.105	
6	220.3	0.000		229.3	0.000	
	235.0	0.000		248.3	0.000	
7	250.9	0.000		265.6	0.000	
	255.6	0.000		272.4	0.000	
	11.911	11.911			13.154	
8	271.9	0.000		283.1	0.000	
	291.9	0.000		303.9	0.000	
	13.582	13.582			11.130	
9	303.1	0.000		307.1	0.000	
	309.5	0.000		315.1	0.000	
	16.153	16.153			13.931	

Table S2. Wave functions with definite projection of the total moment $|m_J\rangle$ for the lowest several spin-orbit states of individual Ln^{III} fragments of **1** and **2** using CASSCF/RASSI-SO with OpenMolcas.

	E/cm^{-1}	wave functions
1_Dy1	0.0	94.8% ±15/2>
	113.4	92.9% ±13/2>
	251.4	70.7% ±11/2>+15.2% ±7/2>+5.4% ±3/2>
1_Dy2	0.0	94.4% ±15/2>
	103.9	91.3% ±13/2>
	236.4	64.5% ±11/2>+16.9% ±7/2>+7.5% ±3/2>
2_Ho1	0.0	76% ±8>+12.2% ±6>+6% ±4>
	2.4	
2_Ho2	0.0	74.6% ±8>+12.6% ±6>+6.8% ±4>
	3.6	

To fit the exchange interactions between Ln^{III} ions in complexes **1** and **2**, we took two steps to obtain them. Firstly, we calculated individual Ln^{III} fragments using CASSCF/RASSI-SO to obtain the corresponding magnetic properties. Then, the exchange interaction between the magnetic centers was considered within the Lines model,^{S7} while the account of the dipole-dipole magnetic coupling is treated exactly.

The Lines model is effective and has been successfully used widely in the research field of $3d$ and $4f$ -elements single-molecule magnets.^{S8, S9}

For complexes **1** and **2**, there is only one type of the effective exchange coupling constant of $\%$. The Ising exchange Hamiltonian is:

$$\hat{H}_{exch} = -\tilde{J}\hat{\vec{S}}_{Ln1}\hat{\vec{S}}_{Ln2} \quad (\text{Ln} = \text{Dy}^{\text{III}} \text{ for } \mathbf{1} \text{ and } \text{Ho}^{\text{III}} \text{ for } \mathbf{2}) \quad (\text{S1})$$

where $\tilde{J} = 25J \cos \alpha$ for **1** and $\tilde{J} = 16J \cos \alpha$ for **2**, α is the angle between the anisotropy axes on sites Ln1 and Ln2, and J is the Lines exchange coupling parameter.

The $\tilde{S}_{Dy} = \tilde{S}_{Ho} = 1/2$ is the ground pseudospin on the Dy^{III} sites and Ho^{III} sites. The total \tilde{J}_{total} is the parameter of the total magnetic interaction ($\tilde{J}_{total} = \tilde{J}_{dipolar} + \tilde{J}_{exchange}$) between magnetic center ions. The dipolar magnetic couplings can be calculated exactly, while the Lines exchange coupling constants were fitted through comparison of the computed and measured magnetic susceptibilities using the POLY_ANISO program.^{S4–S6}

Table S3. Exchange energies E (cm^{-1}), the energy differences between each exchange doublet Δ_t (cm^{-1}) and the main values of the g_z for the lowest two exchange doublets of **1** and **2**.

	1			2		
exchange doublets	E	Δ_t	g_z	E	Δ_t	g_z
1	0.000000000 000	8.786×10^{-8}	18.261	0.000000000 000	2.271×10^0	13.325
	0.000000087 862			2.271276782 816		
2	1.493467782 915	2.534×10^{-7}	34.588	3.919492027 030	2.271×10^0	23.918
	1.493468036 275			6.190756907 062		

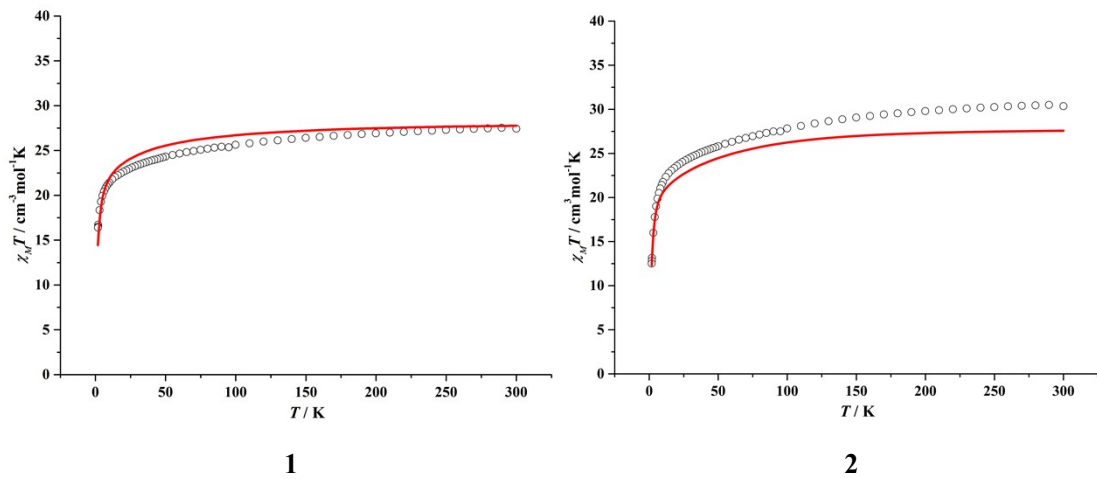


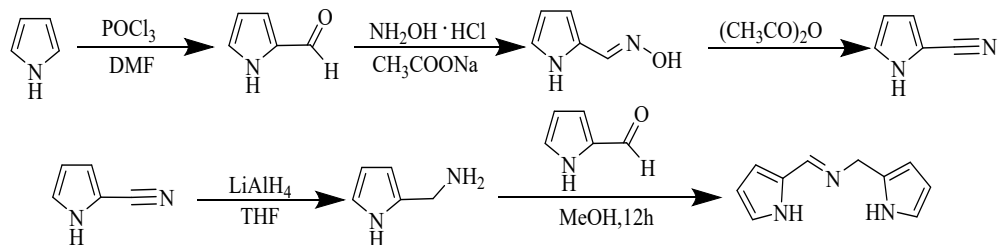
Figure S2. Calculated (red solid line) and experimental (black circle) data of magnetic susceptibilities of **1** and **2**. The intermolecular interaction parameters zJ' of **1** and **2** were fitted to -0.05 and 0.02 cm^{-1} , respectively.

Table S4. Angles between the main magnetic axes on Ln^{III} ions and connection between two metal centers for **1** and **2**.

	1	2
φ_1	109.9°	74.2°
φ_2	108.5°	106.6°

3. Synthesis of the H₂L ligand

Scheme S1. Synthesis of H₂L^{S10}



H₂L. ¹H NMR (300 MHz, CDCl₃) δ 8.35 (s, 1H), 8.13 (s, 1H), 6.79 (s, 1H), 6.70 (s, 1H), 6.52 (d, J = 2.4 Hz, 1H), 6.19 (d, J = 18.9 Hz, 2H), 6.08 (s, 1H), 4.70 (s, 2H).

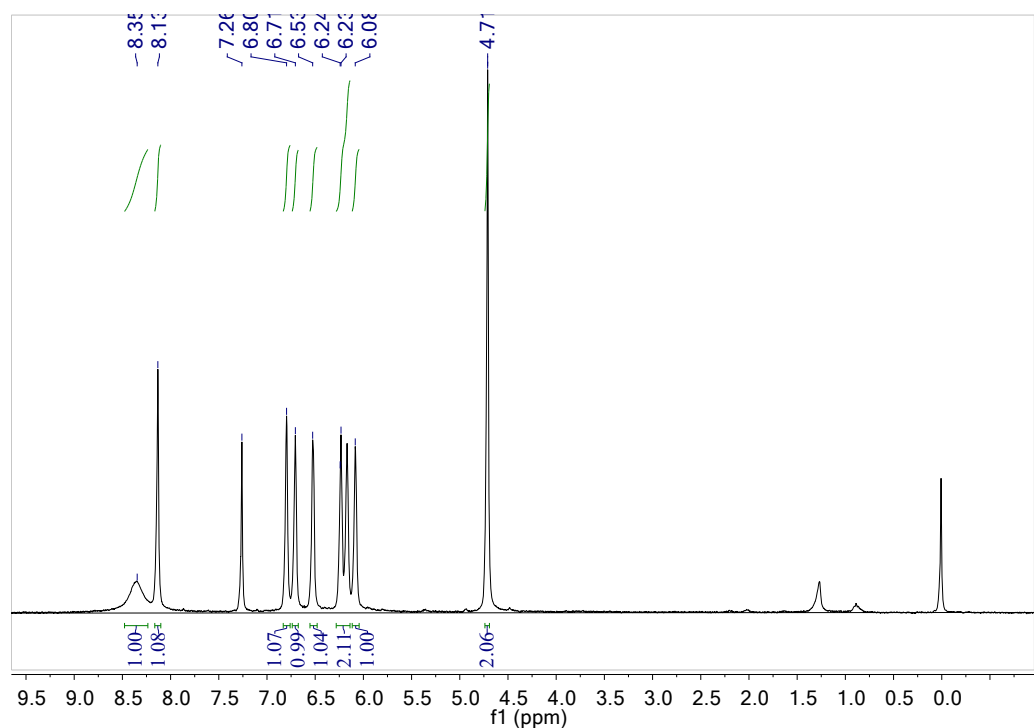


Figure S3. ¹H NMR spectrum of H₂L.

4. Structures and crystallographic data of complexes

4.1. Molecular structures of complexes

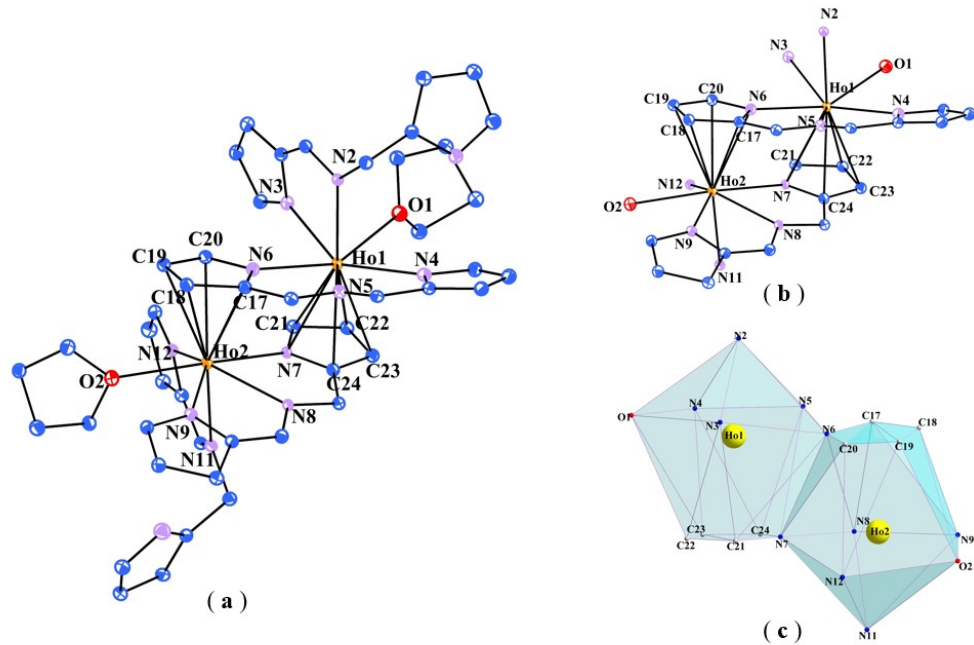


Figure S4. (a) Molecular structure of Complex **2** from X-ray diffraction. Hydrogen atoms are omitted for clarity. Thermal ellipsoids are drawn at the 30% probability level. (b) The central structure of complex **2**. (c) Three-dimensional shapes of the Ho^{III} ions in **2**.

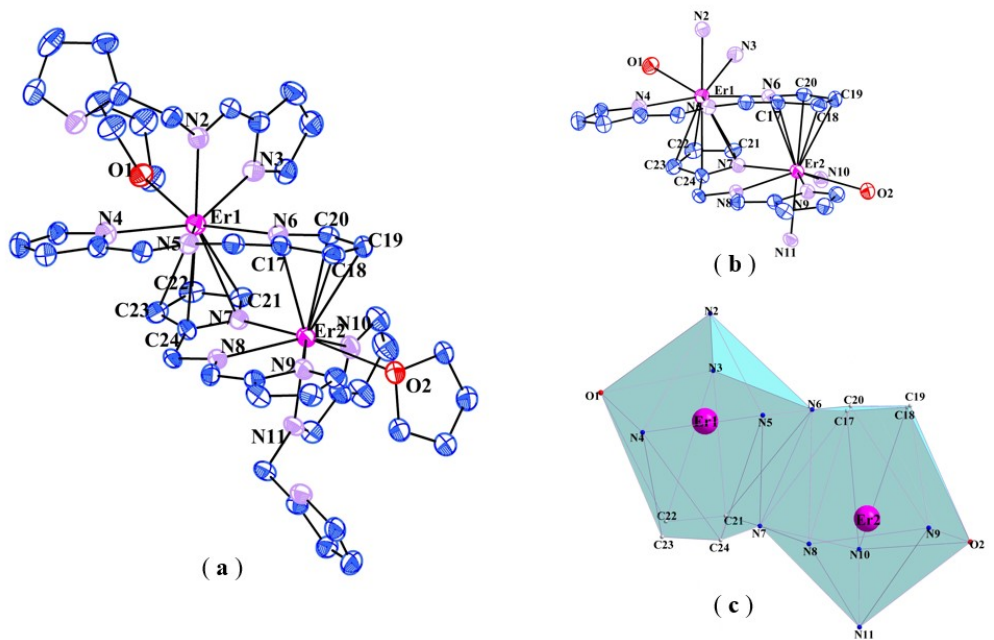


Figure S5. (a)Molecular structure of Complex **3**·4Tol from X-ray diffraction. Hydrogen atoms and solvent molecules are omitted for clarity. Thermal ellipsoids are drawn at the 30% probability level. (b) The core structure of complex **3**·4Tol. (c) Three-dimensional shapes of the Er^{III} ions in **3**·4Tol.

Table S5. Crystallographic data and structure refinement for complexes

	1·2THF	2	3·4Tol
Empirical formula	C ₄₈ H ₅₄ Dy ₂ N ₁₂ O ₂ ·2THF	C ₄₈ H ₅₄ Ho ₂ N ₁₂ O ₂	C ₄₈ H ₅₄ Er ₂ N ₁₂ O ₂ ·4Tol
Formula weight	1300.24	1160.89	1534.08
Crystal system	triclinic	monoclinic	triclinic
Space group	<i>P</i> -1	<i>P</i> 2 ₁ /c	<i>P</i> -1
<i>a</i> /Å	11.5631(4)	14.4788(6)	11.818(4)
<i>b</i> /Å	12.6486(4)	20.2131(8)	17.795(7)
<i>c</i> /Å	19.3347(6)	16.9590(7)	18.503(7)
$\alpha/^\circ$	95.8290(10)	90	76.931(14)
$\beta/^\circ$	102.2810(10)	114.2700(10)	72.258(13)
$\gamma/^\circ$	95.0500(10)	90	73.416(13)
Volume/Å ³	2731.30(15)	4524.6(3)	3511(2)
<i>Z</i>	2	4	2
ρ_{calc} g/cm ³	1.581	1.704	1.451
μ/mm^{-1}	2.772	15.926	8.025
<i>F</i> (000)	1308.0	2304.0	1556.0
Crystal size/mm ³	0.19 × 0.18 × 0.15	0.14 × 0.12 × 0.12	0.16 × 0.14 × 0.12
2θ range for data collection/°	4.346 to 55.098	9.238 to 107.95	9.214 to 108.978
	-15 ≤ <i>h</i> ≤ 15	-17 ≤ <i>h</i> ≤ 17	-14 ≤ <i>h</i> ≤ 13,
Index ranges	-16 ≤ <i>k</i> ≤ 16	-24 ≤ <i>k</i> ≤ 24	-21 ≤ <i>k</i> ≤ 21,
	-25 ≤ <i>l</i> ≤ 25	-20 ≤ <i>l</i> ≤ 20	-22 ≤ <i>l</i> ≤ 22
Reflections collected	52314	54230	31178
Independent reflections	12414 [R(int) = 0.0553]	8166 [R(int) = 0.0633]	12582 [R(int) = 0.0782]
Data/restraints/parameters	12414/24/677	8166/0/577	12582/1910/1070
Goodness-of-fit on <i>F</i> ²	1.061	1.078	1.123
Final <i>R</i> indexes [<i>I</i> ≥ 2σ (<i>I</i>)]	<i>R</i> ₁ = 0.0280 w <i>R</i> ₂ = 0.0699	<i>R</i> ₁ = 0.0380 w <i>R</i> ₂ = 0.0989	<i>R</i> ₁ = 0.0713 w <i>R</i> ₂ = 0.1985
Final <i>R</i> indexes [all data]	<i>R</i> ₁ = 0.0323 w <i>R</i> ₂ = 0.0745	<i>R</i> ₁ = 0.0387 w <i>R</i> ₂ = 0.0995	<i>R</i> ₁ = 0.0884, w <i>R</i> ₂ = 0.2183
Largest diff. peak/hole/e Å ⁻³	1.15/-0.87	1.90/-1.90	1.12/-1.68

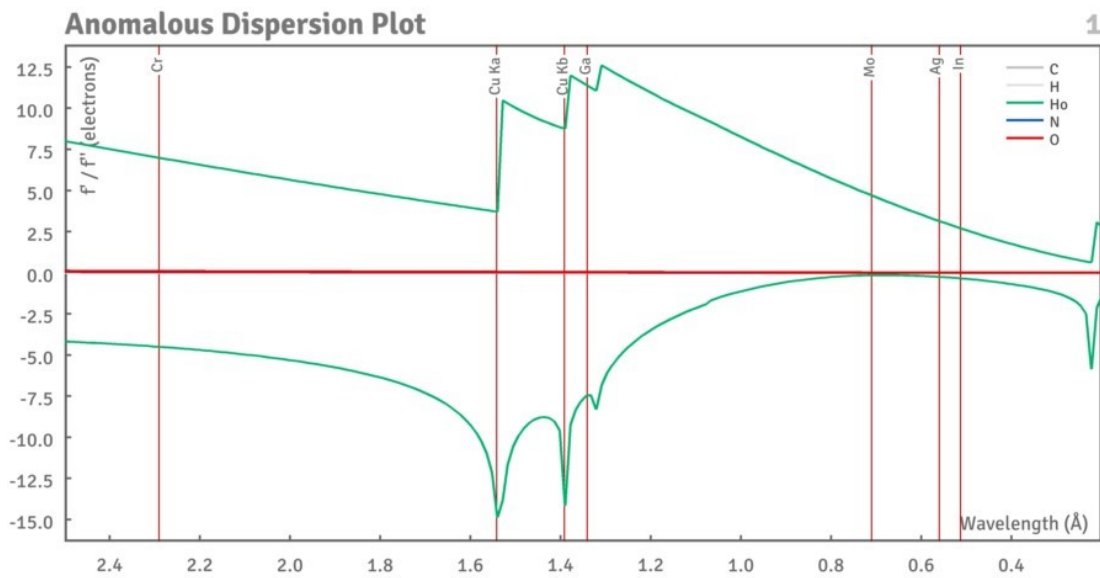


Figure S6. The Anomalous Dispersion plot of complex **2**.

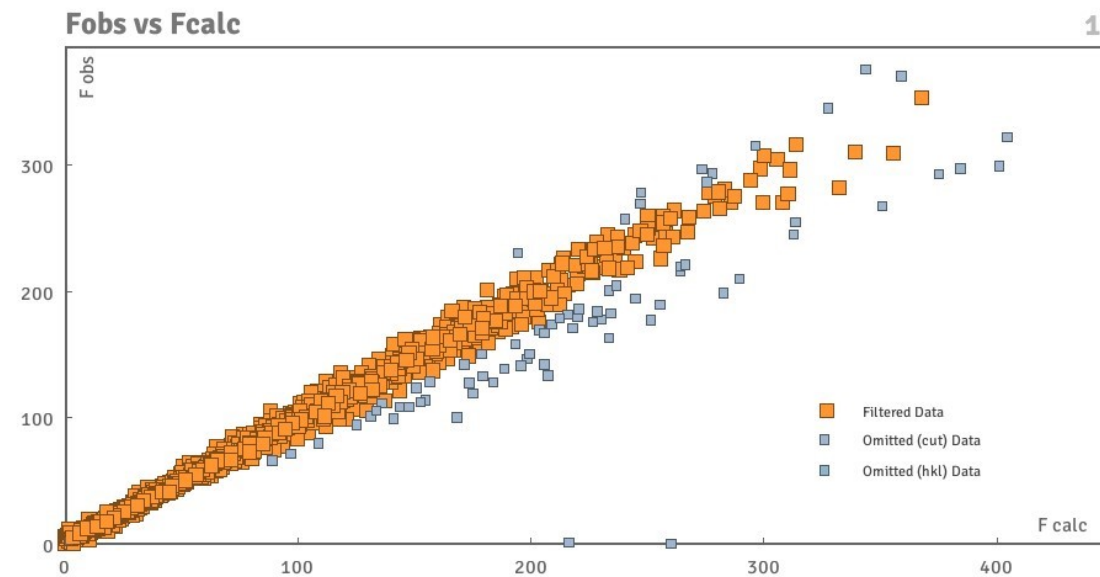


Figure S7. The F_{obs} vs F_{calc} plot of complex **2**.

According to Figure S6, it is not the optimal choice to test with Ga radiation, but the instrument only has Ga radiation at the time of testing, so choose it for testing. Figure S7 is the F_{obs} vs F_{calc} plot of complex **2**, the compound **2** crystal is difficult to cultivate, although the tested crystal is the best one among all the crystals selected, but the crystal data isn't great, and the reduction data have been tried for many times, the effect is not very ideal.

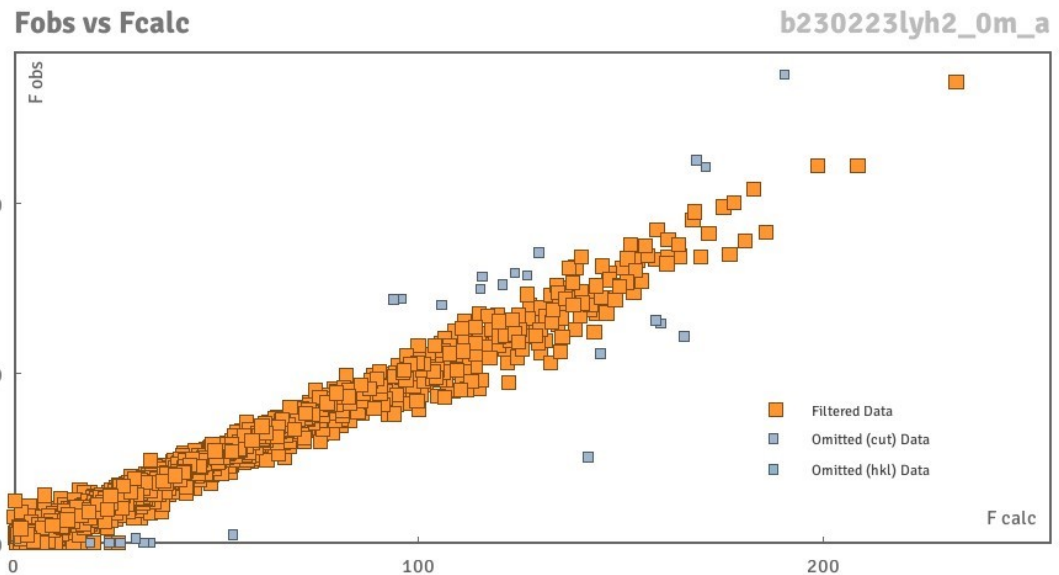


Figure S8. The Fobs vs Fcalc plot of complex **3·4Tol**.

Figure S8 is the Fobs vs Fcalc plot of complex **3·4Tol**. For the data of complex **3·4Tol**: Under the same test conditions, we tested three times and obtained the above data.

4.2. Bond lengths of complexes

Table S6. Selected bond length data

1·2THF					
Dy1-O1	2.533(3)	Dy1-N2	2.470(3)	Dy1-C30	2.741(4)
Dy1-N4	2.460(3)	Dy1-N6	2.431(3)	Dy1-C28	2.812(4)
Dy1-C29	2.808(4)	Dy1-C27	2.745(4)	Dy1-N5	2.495(3)
Dy1-N9	2.722(3)	Dy1-N1	2.408(3)	Dy2-C12	2.828(4)
Dy2-N4	2.704(3)	Dy2-N10	2.409(3)	Dy2-N11	2.474(3)
Dy2-O2	2.542(3)	Dy2-C13	2.825(4)	Dy2-C14	2.746(4)
Dy2-N8	2.494(3)	Dy2-C11	2.730(4)	Dy2-N9	2.471(3)
Dy2-N7	2.420(3)				
2					
Ho2-N12	2.399(3)	Ho2-O2	2.510(3)	Ho2-N7	2.443(3)
Ho2-N6	2.720(3)	Ho2-C18	2.798(4)	Ho2-N11	2.478(3)
Ho2-N9	2.440(3)	Ho2-C17	2.736(4)	Ho2-N8	2.501(3)
Ho2-C20	2.740(4)	Ho2-C19	2.809(4)	Ho1-N7	2.726(3)
Ho1-N2	2.447(3)	Ho1-N6	2.432(3)	Ho1-N5	2.481(3)
Ho1-N3	2.407(3)	Ho1-O1	2.589(3)	Ho1-C21	2.721(3)
Ho1-N4	2.432(3)	Ho1-C23	2.771(4)	Ho1-C22	2.762(4)
Ho1-C24	2.738(3)				

3-4Tol

Er1-O1	2.533(4)	Er1-N2	2.462(5)	Er1-N3	2.385(5)
Er1-N4	2.428(5)	Er1-N5	2.469(6)	Er1-N6	2.439(5)
Er1-N7	2.718(5)	Er1-C21	2.754(7)	Er1-C22	2.789(7)
Er1-C23	2.773(7)	Er1-C24	2.726(6)	Er2-O2	2.519(4)
Er2-N6	2.744(5)	Er2-N7	2.444(5)	Er2-N8	2.458(5)
Er2-N9	2.413(6)	Er2-N10	2.386(6)	Er2-N11	2.444(5)
Er2-C17	2.742(7)	Er2-C18	2.765(7)	Er2-C19	2.797(7)
Er2-C20	2.748(6)				

4.3. Bond Angles of Complexes**Table S7. Selected bond angle data****1-2THF**

N2-Dy1-O1	81.17(8)	N2-Dy1-N9	150.49(8)	N2-Dy1-C29	153.26(9)
N2-Dy1-C30	148.89(8)	N2-Dy1-C27	158.76(9)	N2-Dy1-C28	160.17(9)
N2-Dy1-N5	78.86(8)	N4-Dy1-N2	81.40(8)	N4-Dy1-O1	147.90(7)
N4-Dy1-N9	69.13(7)	N4-Dy1-C29	112.89(8)	N4-Dy1-C30	84.01(8)
N4-Dy1-C27	89.85(8)	N4-Dy1-C28	116.81(8)	N4-Dy1-N5	64.64(8)
O1-Dy1-N9	123.64(7)	O1-Dy1-C29	75.18(8)	O1-Dy1-C30	97.55(8)
O1-Dy1-C27	114.77(8)	O1-Dy1-C28	85.77(8)	N9-Dy1-C29	48.68(8)
N9-Dy1-C30	29.16(8)	N9-Dy1-C27	29.23(7)	N9-Dy1-C28	48.65(8)
C29-Dy1-C28	29.11(9)	N1-Dy1-N2	70.83(9)	N1-Dy1-N4	76.28(8)
N1-Dy1-O1	72.61(8)	N1-Dy1-N9	99.60(8)	N1-Dy1-C29	90.10(9)
N1-Dy1-C30	79.09(9)	N1-Dy1-C27	125.90(9)	N1-Dy1-N6	143.71(8)
N1-Dy1-C28	119.20(9)	N1-Dy1-N5	133.39(8)	C30-Dy1-C29	29.14(9)
C30-Dy1-C27	47.26(8)	C30-Dy1-C28	47.76(9)	C27-Dy1-C29	47.72(9)
C27-Dy1-C28	29.01(8)	N6-Dy1-N2	88.93(8)	N6-Dy1-N4	131.50(8)
N6-Dy1-O1	74.77(8)	N6-Dy1-N9	111.57(8)	N6-Dy1-C29	96.61(9)
N6-Dy1-C30	120.96(9)	N6-Dy1-C27	82.43(8)	N6-Dy1-C28	73.20(9)
N6-Dy1-N5	66.87(8)	N5-Dy1-O1	136.70(8)	N5-Dy1-N9	89.66(8)
N5-Dy1-C29	127.32(9)	N5-Dy1-C30	118.81(8)	N5-Dy1-C27	79.90(8)
N5-Dy1-C28	101.14(9)	O2-Dy2-N4	122.77(7)	O2-Dy2-C13	84.55(8)
O2-Dy2-C12	74.36(8)	O2-Dy2-C11	96.76(7)	O2-Dy2-C14	113.39(7)
N11-Dy2-O2	80.92(7)	N11-Dy2-N4	152.68(7)	N11-Dy2-C13	157.79(8)
N11-Dy2-C12	153.04(8)	N11-Dy2-C11	150.74(8)	N11-Dy2-N9	83.44(8)
N11-Dy2-C14	158.43(8)	N11-Dy2-N8	78.26(8)	N7-Dy2-O2	74.57(7)
N7-Dy2-N11	86.45(8)	N7-Dy2-N4	111.49(8)	N7-Dy2-C13	73.50(9)
N7-Dy2-C12	97.03(9)	N7-Dy2-C11	121.29(8)	N7-Dy2-N9	131.38(8)
N7-Dy2-C14	82.34(9)	N7-Dy2-N8	66.88(8)	N4-Dy2-C13	48.57(8)
N4-Dy2-C12	48.55(8)	N4-Dy2-C11	29.39(7)	N4-Dy2-C14	29.28(8)

C13-Dy2-C12	29.04(9)	C11-Dy2-C13	47.80(9)	C11-Dy2-C12	29.00(9)
C11-Dy2-C14	47.45(9)	N9-Dy2-O2	148.63(7)	N9-Dy2-N4	69.24(7)
N9-Dy2-C13	116.92(8)	N9-Dy2-C12	112.70(8)	N9-Dy2-C11	83.97(8)
N9-Dy2-C14	90.22(8)	N9-Dy2-N8	64.50(8)	C14-Dy2-C13	28.84(8)
C14-Dy2-C12	47.52(8)	N10-Dy2-O2	73.25(7)	N10-Dy2-N11	71.26(8)
N10-Dy2-N7	143.17(8)	N10-Dy2-N4	100.80(8)	N10-Dy2-C13	120.19(8)
N10-Dy2-C12	91.15(8)	N10-Dy2-C11	80.11(8)	N10-Dy2-N9	76.02(8)
N10-Dy2-C14	127.13(8)	N10-Dy2-N8	132.21(8)	N8-Dy2-O2	136.91(7)
N8-Dy2-N4	89.76(7)	N8-Dy2-C13	101.72(9)	N8-Dy2-C12	127.69(8)
N8-Dy2-C11	119.15(8)	N8-Dy2-C14	80.40(8)		

2

O1-Ho1-N7	125.91(9)	O1-Ho1-C21	99.54(10)	O1-Ho1-C22	77.39(10)
O1-Ho1-C23	88.65(10)	O1-Ho1-C24	117.71(10)	N2-Ho1-O1	80.10(9)
N2-Ho1-N5	79.63(9)	N2-Ho1-N7	148.81(9)	N2-Ho1-C21	148.12(10)
N2-Ho1-C22	154.25(11)	N2-Ho1-C23	161.30(10)	N2-Ho1-C24	157.64(10)
N3-Ho1-O1	71.84(9)	N3-Ho1-N2	70.89(10)	N3-Ho1-N4	140.86(10)
N3-Ho1-N5	134.57(10)	N3-Ho1-N6	77.13(10)	N3-Ho1-N7	99.01(9)
N3-Ho1-C21	78.68(11)	N3-Ho1-C22	90.19(11)	N3-Ho1-C23	119.74(11)
N3-Ho1-C24	125.64(10)	N4-Ho1-O1	72.97(10)	N4-Ho1-N2	86.72(10)
N4-Ho1-N5	67.49(11)	N4-Ho1-N6	131.99(11)	N4-Ho1-N7	115.39(9)
N4-Ho1-C21	123.98(11)	N4-Ho1-C22	98.41(11)	N4-Ho1-C23	75.67(10)
N4-Ho1-C24	86.12(10)	N5-Ho1-O1	136.22(9)	N5-Ho1-N7	88.63(9)
N5-Ho1-C21	117.67(10)	N5-Ho1-C22	125.69(10)	N5-Ho1-C23	98.92(10)
N5-Ho1-C24	78.06(10)	N6-Ho1-O1	147.65(9)	N6-Ho1-N2	81.37(10)
N6-Ho1-N5	64.66(10)	N6-Ho1-N7	67.51(9)	N6-Ho1-C21	82.87(10)
N6-Ho1-C22	112.07(11)	N6-Ho1-C23	115.09(10)	N6-Ho1-C24	87.79(10)
N7-Ho1-C22	48.89(10)	N7-Ho1-C23	48.87(10)	N7-Ho1-C24	29.31(10)
C21-Ho1-N7	29.05(10)	C21-Ho1-C22	29.59(11)	C21-Ho1-C23	48.39(11)
C21-Ho1-C24	47.49(11)	C22-Ho1-C23	29.56(11)	C24-Ho1-C22	48.04(11)
C24-Ho1-C23	29.07(11)	O2-Ho2-N6	124.11(9)	O2-Ho2-C17	115.01(10)
O2-Ho2-C18	85.73(11)	O2-Ho2-C19	75.85(10)	O2-Ho2-C20	98.25(10)
N6-Ho2-C17	29.08(10)	N6-Ho2-C18	48.74(10)	N6-Ho2-C19	48.40(10)
N6-Ho2-C20	29.09(10)	N7-Ho2-O2	150.33(9)	N7-Ho2-N6	67.48(9)
N7-Ho2-N8	64.43(10)	N7-Ho2-N11	78.14(10)	N7-Ho2-C17	87.65(10)
N7-Ho2-C18	115.05(11)	N7-Ho2-C19	111.51(11)	N7-Ho2-C20	82.95(11)
N8-Ho2-O2	135.81(9)	N8-Ho2-N6	88.91(9)	N8-Ho2-C17	78.63(10)
N8-Ho2-C18	99.83(12)	N8-Ho2-C19	125.96(11)	N8-Ho2-C20	118.00(10)
N9-Ho2-O2	71.74(9)	N9-Ho2-N6	116.88(9)	N9-Ho2-N7	130.99(10)
N9-Ho2-N8	66.85(10)	N9-Ho2-N11	86.79(10)	N9-Ho2-C17	87.89(10)
N9-Ho2-C18	77.96(12)	N9-Ho2-C19	100.72(12)	N9-Ho2-C20	125.81(11)

N11-Ho2-O2	85.65(9)	N11-Ho2-N6	145.57(10)	N11-Ho2-N8	77.49(9)
N11-Ho2-C17	155.71(11)	N11-Ho2-C18	164.22(11)	N11-Ho2-C19	156.50(11)
N11-Ho2-C20	146.85(11)	N12-Ho2-O2	73.87(10)	N12-Ho2-N6	99.46(10)
N12-Ho2-N7	77.30(10)	N12-Ho2-N8	134.04(10)	N12-Ho2-N9	139.77(10)
N12-Ho2-N11	70.31(10)	N12-Ho2-C17	125.86(11)	N12-Ho2-C18	119.60(12)
N12-Ho2-C19	90.43(12)	N12-Ho2-C20	79.15(11)	C17-Ho2-C18	29.28(12)
C17-Ho2-C19	47.68(12)	C17-Ho2-C20	47.24(12)	C18-Ho2-C19	29.17(13)
C20-Ho2-C18	47.91(13)	C20-Ho2-C19	28.97(12)		

3·4Tol

O1-Er1-N7	125.50(15)	O1-Er1-C21	100.38(17)	O1-Er1-C22	76.85(18)
O1-Er1-C23	84.85(18)	O1-Er1-C24	114.27(17)	N2-Er1-O1	80.95(17)
N2-Er1-N5	76.87(18)	N2-Er1-N7	150.11(16)	N2-Er1-C21	148.98(19)
N2-Er1-C22	153.57(19)	N2-Er1-C23	160.1(2)	N2-Er1-C24	158.45(19)
N3-Er1-O1	72.88(17)	N3-Er1-N2	71.31(19)	N3-Er1-N4	143.26(18)
N3-Er1-N5	132.57(19)	N3-Er1-N6	76.81(18)	N3-Er1-N7	101.13(17)
N3-Er1-C21	79.4(2)	N3-Er1-C22	88.5(2)	N3-Er1-C23	117.5(2)
N3-Er1-C24	126.43(19)	N4-Er1-O1	73.45(17)	N4-Er1-N2	89.28(18)
N4-Er1-N5	67.90(17)	N4-Er1-N6	132.56(18)	N4-Er1-N7	110.17(17)
N4-Er1-C21	121.03(19)	N4-Er1-C22	97.8(2)	N4-Er1-C23	73.3(2)
N4-Er1-C24	81.24(18)	N5-Er1-O1	135.20(17)	N5-Er1-N7	89.38(16)
N5-Er1-C21	118.42(18)	N5-Er1-C22	129.36(19)	N5-Er1-C23	104.3(2)
N5-Er1-C24	81.63(19)	N6-Er1-O1	148.77(16)	N6-Er1-N2	82.41(17)
N6-Er1-N5	64.72(18)	N6-Er1-N7	67.71(16)	N6-Er1-C21	81.11(19)
N6-Er1-C22	110.0(2)	N6-Er1-C23	116.36(18)	N6-Er1-C24	89.79(17)
N7-Er1-C21	29.11(17)	N7-Er1-C22	48.66(18)	N7-Er1-C23	49.03(18)
N7-Er1-C24	29.16(17)	C21-Er1-C22	29.0(2)	C21-Er1-C23	47.8(2)
C23-Er1-C22	29.1(2)	C24-Er1-C21	47.1(2)	C24-Er1-C22	47.77(19)
C24-Er1-C23	29.49(19)	O2-Er2-N6	126.53(15)	O2-Er2-C17	115.68(17)
O2-Er2-C18	85.88(18)	O2-Er2-C19	77.79(17)	O2-Er2-C20	101.23(17)
N6-Er2-C18	48.96(18)	N6-Er2-C19	48.75(17)	N6-Er2-C20	29.42(18)
N7-Er2-O2	148.27(17)	N7-Er2-N6	67.22(16)	N7-Er2-N8	64.99(17)
N7-Er2-N11	81.81(17)	N7-Er2-C17	89.00(18)	N7-Er2-C18	115.84(19)
N7-Er2-C19	109.48(18)	N7-Er2-C20	80.32(19)	N8-Er2-O2	134.88(15)
N8-Er2-N6	89.09(16)	N8-Er2-C17	81.16(18)	N8-Er2-C18	104.2(2)
N8-Er2-C19	129.19(19)	N8-Er2-C20	118.39(18)	N9-Er2-O2	73.39(17)
N9-Er2-N6	110.68(17)	N9-Er2-N7	132.78(18)	N9-Er2-N8	67.82(17)
N9-Er2-N11	89.16(18)	N9-Er2-C17	82.04(19)	N9-Er2-C18	74.0(2)
N9-Er2-C19	98.4(2)	N9-Er2-C20	122.1(2)	N10-Er2-O2	72.68(17)
N10-Er2-N6	101.66(17)	N10-Er2-N7	76.54(18)	N10-Er2-N8	132.13(18)
N10-Er2-N9	142.75(19)	N10-Er2-N11	70.83(19)	N10-Er2-C17	126.96(19)
N10-Er2-C18	118.0(2)	N10-Er2-C19	89.1(2)	N10-Er2-C20	79.6(2)
N11-Er2-O2	81.05(16)	N11-Er2-N6	149.01(16)	N11-Er2-N8	76.31(18)
N11-Er2-C17	157.47(19)	N11-Er2-C18	161.12(19)	N11-Er2-C19	154.4(2)

N11-Er2-C20	148.2(2)	C17-Er2-N6	28.86(17)	C17-Er2-C18	29.88(19)
C17-Er2-C19	48.1(2)	C17-Er2-C20	47.6(2)	C18-Er2-C19	29.0(2)
C20-Er2-C18	48.2(2)	C20-Er2-C19	29.3(2)		

5. SHAPE program details for 1·2THF, 2, and 3·4Tol

Table S8. Shape analysis for eleven-coordinated Ln^{III} ions of complexes 1·2THF, 2, and 3·4Tol

Agreement factor for Ln ^{III} ions in complexes	<i>HP</i> -11	<i>DPY</i> -11	<i>EBPY</i> -11	<i>JCPPR</i> -11	<i>JCPAPR-</i> 11	<i>JAPPR</i> -11	<i>JASPC</i> -11
Dy1 ^{III} in 1·2THF	36.376	26.640	21.942	11.062	13.167	15.816	16.191
Dy2 ^{III} in 1·2THF	36.661	26.553	21.869	10.992	13.222	15.943	16.220
Ho1 ^{III} in 2	36.303	26.697	21.939	10.701	13.214	16.444	16.284
Ho2 ^{III} in 2	35.700	26.302	21.763	10.947	13.235	15.953	16.460
Er1 ^{III} in 3·4Tol	36.351	26.627	21.645	11.419	12.657	15.785	15.857
Er2 ^{III} in 3·4Tol	36.172	26.582	21.569	11.258	12.618	15.783	15.829

HP-11 (D_{11h}) = Hendecagon, *DPY*-11 (C_{10v}) = Decagonal pyramid, *EBPY*-11 (D_{9h}) = Enneagonal bipyramid, *JCPPR*-11 (C_{5v}) = Capped pentagonal prism, *JCPAPR*-11 (C_{5v}) = Capped pentagonal antiprism, *JAPPR*-11 (C_{2v}) = Augmented pentagonal prism, *JASPC*-11(C_s) = Augmented sphenocorona.

6. The AC magnetic susceptibility measurement of complexes 1 and 2

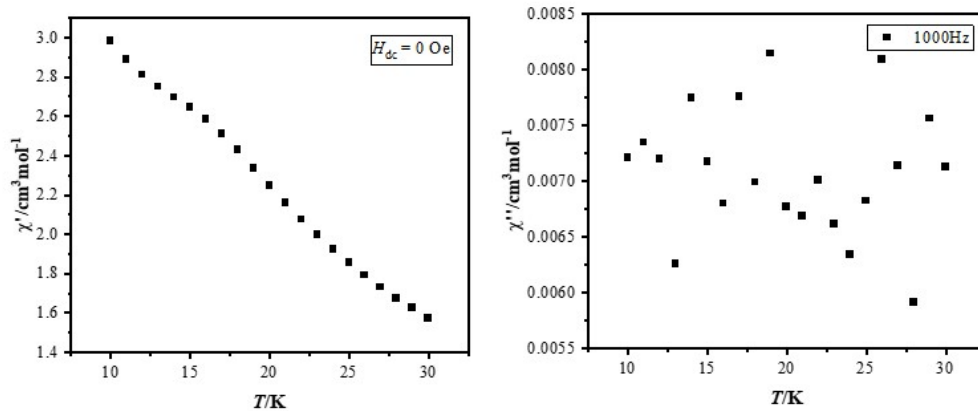


Figure S9. Temperature dependence of the in-phase χ' (left) and out-of-phase χ'' (right) susceptibilities for complex 1 at 0 Oe dc field and the frequency of 1000 Hz between 10 and 30 K.

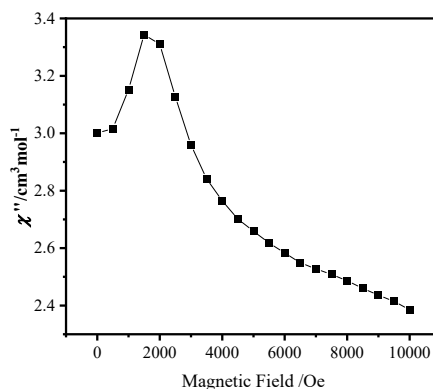


Figure S10. Magnetic field dependence of the out-of-phase (χ'') susceptibilities for 1 in the 0–10000 Oe dc field (at temperature of 10 K and frequency of 1000 Hz).

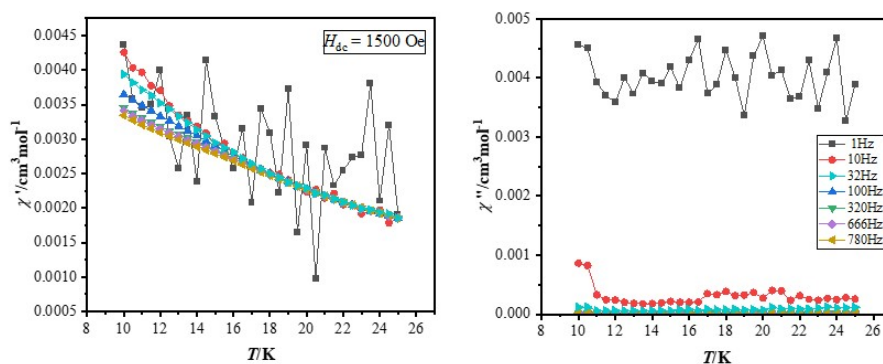


Figure S11. Temperature dependence of the in-phase χ' (left) and out-of-phase χ'' (right) susceptibilities for complex 1 at 1500 Oe dc field between 10 and 25 K.

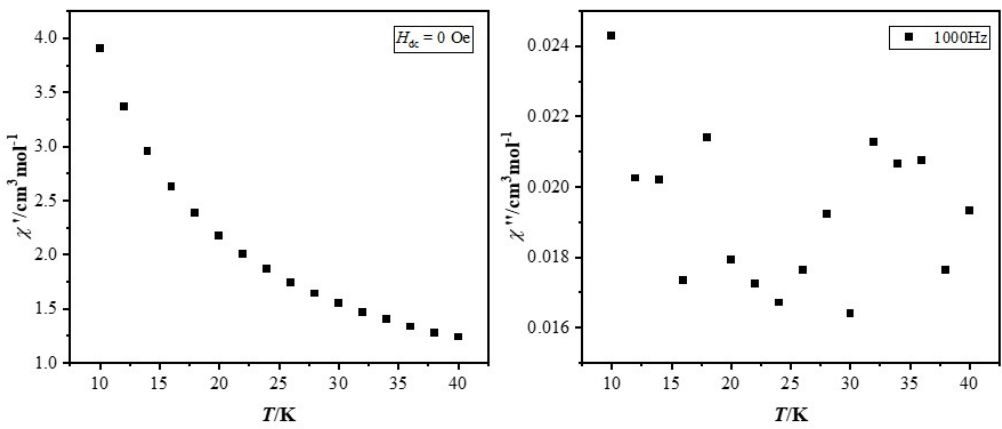


Figure S12. Temperature dependence of the in-phase χ' (left) and out-of-phase χ'' (right) susceptibilities for complex **2** at 0 Oe dc field and the frequency of 1000 Hz between 10 and 40 K.

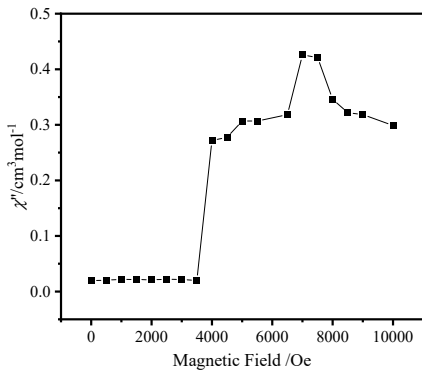


Figure S13. Magnetic field dependence of the out-of-phase (χ'') susceptibilities for **2** in the 0-10000 Oe dc field (at temperature of 10 K and frequency of 1000 Hz).

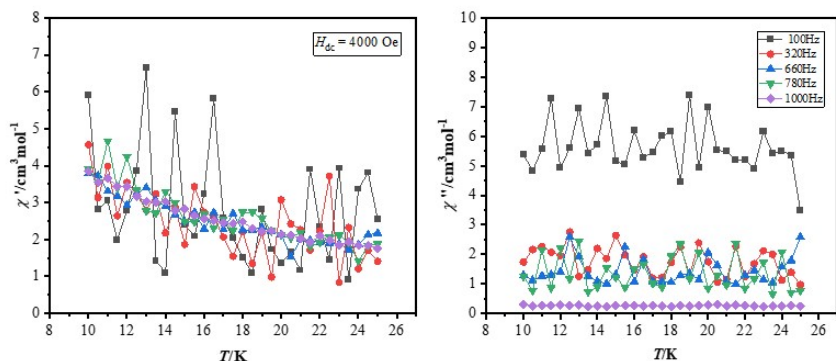


Figure S14. Temperature dependence of the in-phase χ' (left) and out-of-phase χ'' (right) susceptibilities for complex **2** at 4000 Oe dc field between 10 and 25 K.

7. The M - H plots of complexes 1-4.

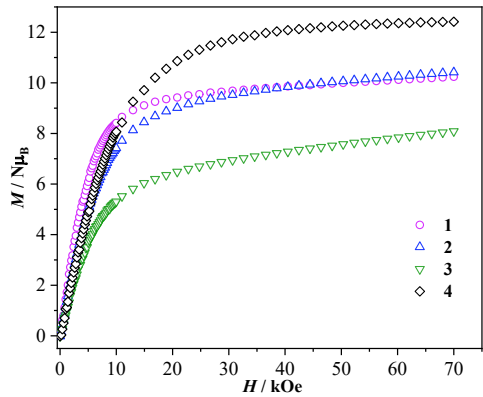


Figure S15. M - H plots for complexes 1 ~ 4 at 2 K.

8. The Curie-Weiss law fits of complexes 1-4.

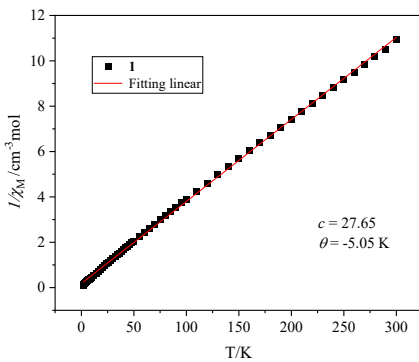


Figure S16. Plot of $1/\chi_M$ versus T for **1** and the linear fits represent the Curie-Weiss law fit at 1 kOe field.

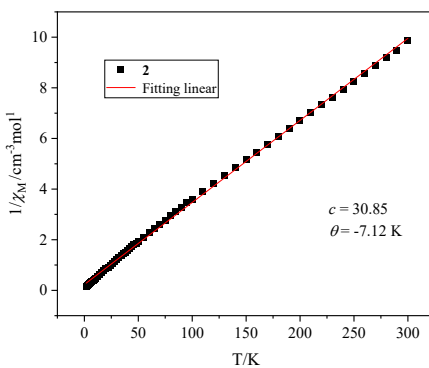


Figure S17. Plot of $1/\chi_M$ versus T for **2** and the linear fits represent the Curie-Weiss law fit at 1 kOe field.

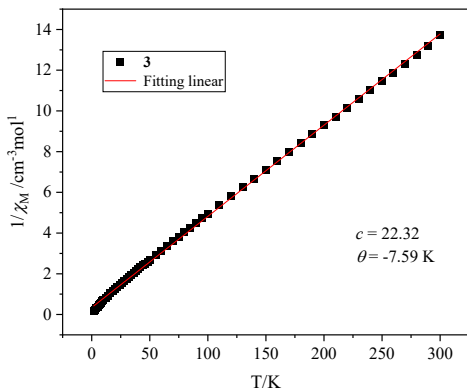


Figure S18. Plot of $1/\chi_M$ versus T for **3** and the linear fits represent the Curie-Weiss law fit at 1 kOe field.

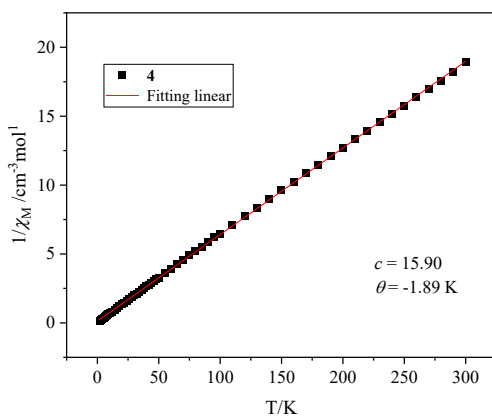


Figure S19. Plot of $1/\chi_M$ versus T for **4** and the linear fits represent the Curie-Weiss law fit at 1 kOe field.

References:

- [1] F. Galván, M. Vacher, A. Alavi, C. Angeli, F. Aquilante, J. Autschbach, J. J. Bao, S. I. Bokarev, N. A. Bogdanov, R. K. Carlson, L. F. Chibotaru, J. Creutzberg, N. Dattani, M. G. Delcey, S. S. Dong, A. Dreuw, L. Freitag, L. M. Frutos, L. Gagliardi, F. Gendron, A. Giussani, L. González, G. Grell, M. Y. Guo, C. E. Hoyer, M. Johansson, S. Keller, S. Knecht, G. Kovacevic, E. Källman, G. L. Manni, M. Lundberg, Y. J. Ma, S. Mai, J. P. Malhado, P. Å. Malmqvist, P. Marquetand, S. A. Mewes, J. Norell, M. Olivucci, M. Oppel, Q. M. Phung, K. Pierloot, F. Plasser, M. Reiher, A. M. Sand, I. Schapiro, P. Sharma, C. J. Stein, L. K. Sørensen, D. G. Truhlar, M. Ugandi, L. Ungur, A. Valentini, S. Vancoillie, V. Veryazov, O. Weser, T. A. Wesołowski, Per-Olof Widmark, S. Wouters,; A. Zech, J. P. Zobel and R. Lindh, *J. Chem. Theory Comput.*, 2019, **15**, 5925-5964.
- [2] P. Å. Malmqvist, B. O. Roos and B. Schimmelpfennig, *Chem. Phys. Lett.*, 2002, **357**, 230-240.
- [3] B. A. Heß, C. M. Marian, U. Wahlgren and O. Gropen, *Chem. Phys. Lett.*, 1996, **251**, 365-371.
- [4] L. F. Chibotaru, L. Ungur and A. Soncini, *Angew. Chem., Int. Ed.*, 2008, **47**, 4126-4129.
- [5] L. Ungur, W. Van den Heuvel and L. F. Chibotaru, *New J. Chem.*, 2009, **33**, 1224-1230.
- [6] L. F. Chibotaru, L. Ungur, C. Aronica, H. Elmoll, G. Pilet and D. Luneau, *J. Am. Chem. Soc.*, 2008, **130**, 12445-12455.
- [7] M. E. Lines, *J. Chem. Phys.*, 1971, **55**, 2977-2984.
- [8] K. C. Mondal, A. Sundt, Y. H. Lan, G. E. Kostakis, O. Waldmann, L. Ungur, L. F. Chibotaru, C. E. Anson and A. K. Powell, *Angew. Chem., Int. Ed.*, 2012, **51**, 7550-7554.
- [9] S. K. Langley, D. P. Wielechowski, V. Vieru, N. F. Chilton, B. Moubaraki, B. F. Abrahams, L. F. Chibotaru and K. S. Murray, *Angew. Chem., Int. Ed.*, 2013, **52**, 12014-12019.
- [10] Y. L. Wang, Y. Dang, H. F. Pan, Y. Ge, Z. L. Jiang, S. W. Xia and Y. H. Li, *Chinese J. Struct. Chem.*, 2019, **38**, 1797-1806.